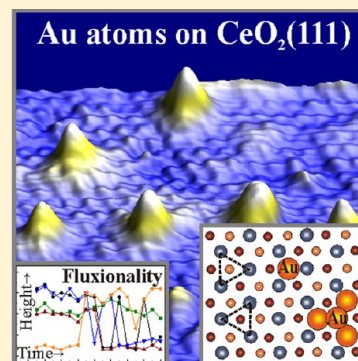


Gold Adsorption on CeO₂ Thin Films Grown on Ru(0001)

Yi Pan,[†] Yi Cui,[†] Christian Stiehler,[†] Niklas Nilus,^{*,†,‡} and Hans-Joachim Freund[†][†]Fritz-Haber-Institut der Max-Planck-Gesellschaft, Faradayweg 4-6, D-14195 Berlin, Germany[‡]Institut für Physik, Carl von Ossietzky Universität Oldenburg, D-26111 Oldenburg, Germany

ABSTRACT: The adsorption of gold has been investigated on crystalline and defect-poor CeO₂(111) films by means of low-temperature scanning tunneling microscopy and spectroscopy. At low coverage, individual Au atoms are observed that homogeneously distribute on the ceria surface and show no preference for binding at step edges. With increasing exposure, characteristic Au aggregates become visible, such as upright Au dimers and bilayer and trilayer pyramids. The ultrasmall clusters exhibit pronounced fluxionality; i.e., they easily modify their internal shape and binding position during the scanning process. This observation suggests the presence of various iso-energetic Au isomers on the surface and points to a relatively weak metal–oxide interaction. At higher Au exposure, tall 3D particles develop on the ceria surface. Conductance spectroscopy on these deposits reveals a set of unoccupied states localized in the energy region of the Au 6p levels. Neither the topographic nor the spectroscopic data indicate a charging of Au species on the defect-poor CeO₂(111) surface, suggesting that Au mainly binds in the neutral charge state.



1. INTRODUCTION

The gold–ceria system has model character for elucidating the interaction between noble metal aggregates and reducible oxides and has therefore been in the focus of research already for several years.¹ The interest is driven by numerous experimental results, which demonstrate that gold and other precious metals supported on crystalline and nanostructured ceria are highly active in technologically relevant processes, such as the water–gas-shift (WGS) reaction² and the ethanol conversion to hydrogen.³ Despite strong experimental efforts, the underlying mechanism is still not well understood, and the proposed models are sometimes in contradiction to each other. For example, while Flytzani-Stephanopoulos and co-workers promote the idea of cationic gold being active in the WGS reaction,^{2,4} Rodriguez et al. provide evidence that mainly neutral gold is involved in the WGS process, and the high dispersion of ceria is a main factor.¹ So far, consensus is reached only in the fact that the catalytic activity of the Au–ceria system is an interface effect, in which the oxide provides suitable sites for water dissociation and enables reverse spillover of oxygen, while the metal stabilizes the CO molecules on the surface. Also, the facile reducibility of ceria is of pivotal importance because it allows for charge transfer from the metal deposits into Ce⁴⁺ ions acting as electron acceptors. However, whether this charge transfer plays a role in chemical reactions over ceria and which structural and electronic requirements are needed for the electron exchange is still subject of discussions.

Due to its practical relevance, the gold–ceria system has been intensively studied by theory as well.^{5,6} One main conclusion was that the interface interaction strength and the associated charge transfer sensitively depend on the computational approach and the exact functional used for calculations. This uncertainty arises from the computational difficulties to describe the highly contracted Ce 4f orbitals and concomitant

electron correlation effects.^{7–9} Consequently, a wide range of theoretical results have been put forward for the binding strength and charge state of individual Au atoms bound to perfect and defective CeO₂ surfaces. The main trends are that Au interacts rather weakly and in a neutral state with stoichiometric CeO₂(111) ($E_{\text{bind}} \sim 1.0$ eV), while reinforced bonding is revealed to surface O-vacancies (~ 2.5 eV) and Ce defects (~ 5.0 eV).^{10,11} In the latter two cases, the adatom either lowers its oxidation state by accepting an electron from a Ce³⁺ ion associated to the O defect or becomes positively charged due to electron transfer into O 2p-like hole states induced by the Ce defect. In small Au clusters, only those atoms that are in direct contact with the oxide defect experience a substantial charge transfer, while the others remain essentially neutral. With regard to chemical reactions, mainly the CO oxidation over ceria-supported Au species has been explored theoretically.¹² The reaction was found to proceed via CO adsorption on the Au atom, oxygen spillover from the ceria surface, and desorption of the CO₂ complex, in agreement with a Mars van Krevelen type of reaction.¹⁵

So far, the different Au–ceria coupling schemes proposed by theory could be verified only in part due to the lack of atomic-scale experiments.¹⁴ By means of scanning tunneling microscopy (STM), the preferred gold nucleation sites were identified to be step edges on stoichiometric oxides but point defects on highly reduced surfaces.^{15,16} The charge state of the ad-gold was deduced indirectly from infrared-reflection-absorption spectroscopy using CO as a probe molecule. From the blue shift in the stretch frequency when dosing CO onto Au aggregates bound to defect-rich versus defect-poor

Received: July 31, 2013

Revised: September 17, 2013

surfaces, the formation of positively charged gold was concluded in the presence of O vacancies. However, no direct correlation between a certain defect type and the occurrence of $\text{Au}^{\delta+}$ species could be given so far, and the origin of cationic gold is still under debate. Note that the charge state of single atoms and small aggregates on oxide surfaces can in principle be determined by means of STM conductance spectroscopy, as demonstrated in refs 17 and 18.

In the present work, we have investigated the nucleation and growth of ultrasmall Au deposits on atomically flat $\text{CeO}_2(111)$ films grown on a Ru(0001) surface. Using low-temperature STM, characteristic Au agglomerates and their binding positions on the surface have been identified, such as monomers, upright dimers, bilayer and trilayer pyramids. Their size-dependent electronic structure was analyzed with the help of STM conductance spectroscopy.

2. EXPERIMENT

All measurements have been performed in a liquid-helium cooled STM setup ($T = 4.5$ K), equipped with standard tools for sample preparation and analysis in ultrahigh vacuum. Imaging was performed in the constant current mode with current values of 5–10 pA to minimize tip–sample interactions. The sample electronic structure was probed with differential conductance (dI/dV) spectroscopy using a lock-in amplifier. The ceria films were prepared by deposition of elemental Ce from a Mo crucible in 1×10^{-6} mbar of O_2 onto a Ru(0001) surface that has been cleaned before with cycles of Ar^+ sputtering and annealing to 1300 K.^{15,19,20} After deposition, the samples were annealed to 1000 K in oxygen and slowly cooled to room temperature. The resulting films displayed a sharp, hexagonal spot pattern with a periodicity of 0.7 times the one of pristine Ru(0001), indicating the formation of crystalline $\text{CeO}_2(111)$. The corresponding STM images showed triangular and hexagonal oxide patches with a mean size of 500 Å and a thickness of 9–15 Å (three to five O–Ce–O trilayers) (Figure 1a). In addition, small areas of bare Ru with a (2×2) O superstructure were observed, developing due to a partial dewetting of the oxide film during the high-temperature annealing. This mixed surface morphology turned out to be beneficial for our experiments because it enabled effective tip-preparation cycles over the metallic parts of the sample.

Atomically resolved STM images were obtained primarily at positive sample bias (empty states) and showed the hexagonal arrangement of Ce^{4+} ions in the surface (Figure 1a).²¹ At this polarity, O vacancies appeared either as double/triple protrusions or as trifoliated depressions, depending on their localization in the topmost²¹ or the second O^{2-} plane, respectively.^{22–24} In the first case, the spill-out of Ce^{4+} wave functions at the defect site is responsible for the enhanced contrast,²⁵ while in the second case, the modified electronic structure in the presence of subsurface vacancies gives rise to a slight reduction of the tunneling probability.^{22,26} Mostly subsurface defects have been detected on our films because the surface defects efficiently heal at our oxygen-rich preparation conditions. The typical concentration of subsurface defects has been determined to be $2.5 \times 10^{12} \text{ cm}^{-2}$ on the basis of atomically resolved images (Figure 1a). Gold deposition was performed inside the cryogenic microscope at a sample temperature of 10 K. The nominal coverage was varied between 0.01 and 0.5 ML, as calibrated with STM imaging.

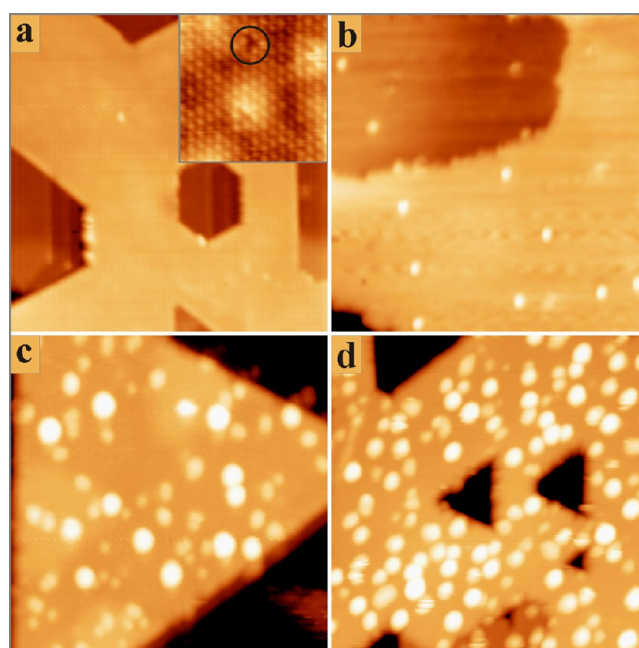


Figure 1. STM topographic images of (a) bare $\text{CeO}_2(111)$ grown on Ru(0001) (3.0 V, $80 \times 80 \text{ nm}^2$) and (b–d) after deposition of increasing amounts of Au at 10 K (3.0 V $45 \times 45 \text{ nm}^2$). As the ceria film dewets from the support upon high-temperature annealing, bare Ru regions with triangular/hexagonal shapes are visible in the images. The thickness of the oxide patches has been determined to be 3–5 O–Ce–O trilayers. The inset in (a) displays the atomically resolved Ce^{4+} lattice with a subsurface oxygen vacancy marked by the circle (0.7 V, $5 \times 5 \text{ nm}^2$).

3. RESULTS AND DISCUSSION

3.1. Binding Position and Geometry of the Au Aggregates. After dosing traces of gold, circular protrusions of 1.5 Å apparent height (at 3.0 V sample bias) appear on the ceria film, which are readily assigned to individual Au atoms (Figure 1b). They are randomly distributed on the surface and show no preference for binding at step edges. This finding suggests limited mobility of the adatoms at the low deposition temperature in our experiment, as Au nucleation mainly along the ceria step edges has been reported in an earlier room-temperature study.¹⁵ Atomically resolved STM images provide insight into the binding site of Au atoms on the $\text{CeO}_2(111)$ surface. In the empty-state image shown in Figure 2a, both the Ce sublattice as well as individual Au species are clearly resolved. The positions of surface O atoms are indirectly derived from the preferred orientation of equilibrium step edges in the $\text{CeO}_2(111)$ surface, as displayed in Figure 1. Using the most favorable step termination (the type-I step edge in ref 27) as internal reference, the right-pointing triangles in the Ce sublattice can be assigned to the O^{2-} surface atoms, while the left-pointing triangles mark the subsurface O^{2-} sites (Figure 2c). This assignment was cross-checked for surface and subsurface defects that indeed occupy the expected lattice positions. With this procedure, two Au adsorption sites were identified on the defect-free $\text{CeO}_2(111)$ terraces. The first one, denoted as T, corresponds to an O-top site, while the second one (marked as B) better fits to a Ce site, but would also be compatible with a nearby bridge position between two surface oxygen ions (Figure 2b). Note that there is an uncertainty in the site determination with STM that relates to the large appearance of single Au atoms in comparison to the oxide

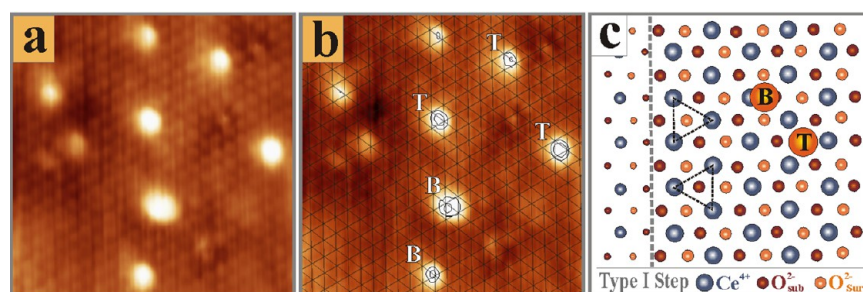


Figure 2. (a) Atomically resolved STM topography of the $\text{CeO}_2(111)$ surface with a couple of Au adatoms ($6.5 \times 6.5 \text{ nm}^2$). (b) The Au binding sites have been determined by overlaying a hexagonal grid for the Ce sublattice and assigning the position of surface and subsurface O^{2-} ions with the help of the orientation of nearby step edges. The derived binding sites for gold correspond to either top (T) or bridge positions (B) with respect to the surface O^{2-} ions.

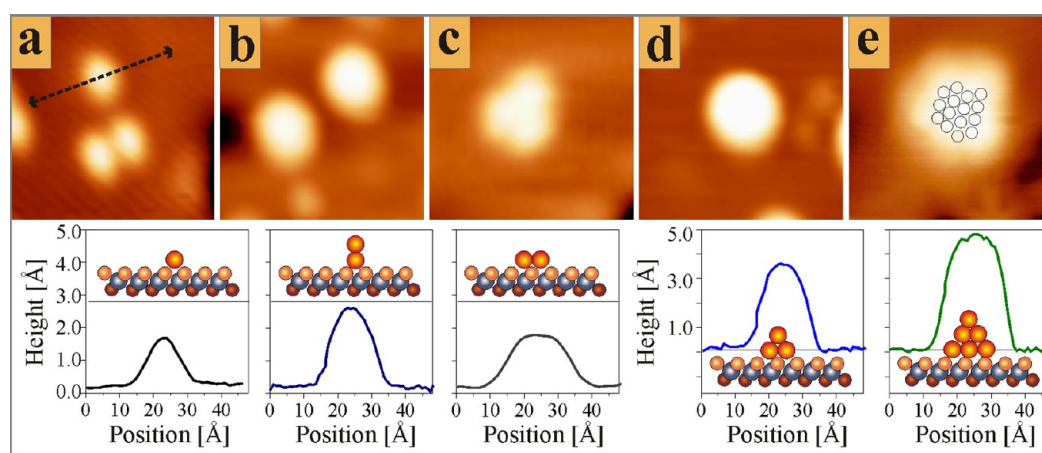


Figure 3. STM topographies of selected Au nanostructures on the $\text{CeO}_2(111)$ surface at low Au exposure. The respective height profiles and structure models are displayed in the lower panels (2.5 V , $5 \times 5 \text{ nm}^2$). (a) Monomers, (b) upright dimers, (c) flat-lying trimer, (d) bilayer pyramid, and (e) trilayer pyramid.

lattice parameter. Both adsorption configurations found in the experiment, O-top and O–O bridge sites, have been considered in theoretical studies as well.^{6,28} Recent GGA+U calculations revealed a slight preference of the bridge position over the top site, although the energy difference was small and dependent on the employed functional. The preference for the bridge site was explained with a minimization of the Pauli repulsion between the Au $6s^1$ and the filled O $2p$ states, combined with an appreciable Au $6sp$ –Ce $4f$ overlap in this configuration.²⁸ We note that the adsorption behavior becomes more complex on defective $\text{CeO}_2(111)$, as both surface and subsurface O vacancies are able to bind the incoming Au atoms. This topic is addressed in a forthcoming paper.

At higher coverage, small Au aggregates appeared next to the isolated monomers on the ceria surface (Figure 1c). We were able to identify a number of distinct configurations by using their apparent height, shape, and diameter as topographic fingerprints. The first species is 70% taller than a single atom (2.5 \AA) but still exhibits a circular base (Figure 3b). It comprises two Au atoms, information that we gained from the direct observation of its formation out of two closely spaced monomers as shown in Figure 3a. We thus conclude that these aggregates are up-right standing dimers. They become favorable if the gold–support interaction is weak and no suitable binding sites are available at the optimal Au–Au distance (2.5 \AA in gas-phase Au_2). Upright-standing Au dimers have been identified on $\text{MgO}(001)$ before,^{29,30} where they developed mainly between neutral Au atoms. In the case of charged species,

flat-lying dimers were found to be preferred, as both adsorbates can couple electrostatically to the oxide surface in this geometry. As upright dimers are the dominant biatomic species on $\text{CeO}_2(111)$, we suggest that charge transfer into or out of the gold is negligible at least on defect-poor films.

In contrast, aggregates containing three atoms mainly adopt planar configurations, as exemplified by the trimer in Figure 3c. Occasionally, flat islands with higher atom numbers, e.g., tetramers and pentamers, were observed as well. Interestingly, the monolayer islands on ceria always featured compact shapes, while mainly 1D cluster geometries have been observed on alumina and magnesia thin films.^{18,31} Linear shapes are usually assigned to electron-rich clusters, as the 1D geometry helps minimize the electron–electron repulsion between the charged atoms. The absence of linear shapes therefore provides another indication for the close-to-neutral charge state of Au species on the ceria surface. A peculiarity of Au aggregation on $\text{CeO}_2(111)$ is the preference for compact 3D shapes, evidenced by the abundance of relatively tall clusters even at low nominal coverage. One typical 3D aggregate is characterized by an apparent height of 3.5 \AA and a diameter of 12 \AA , a geometry that would match a bilayer pyramid with three Au atoms in the bottom and one in the top plane (Figure 3d). At higher exposure, trilayer pyramids of approximately 4.5 \AA height are found as well (Figure 3e). Assuming fcc-type atom packing, those aggregates likely comprise 15, 7, and 3 Au atoms in the bottom, middle, and top layer, respectively.

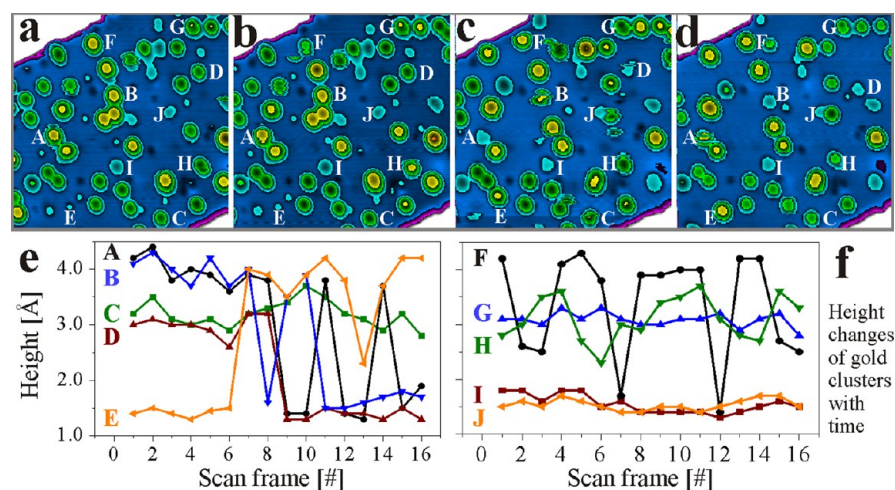


Figure 4. Color-coded representation of Au aggregates of different height on CeO₂(111) (2.8 V, 20 × 20 nm²). Monolayer, bilayer, and trilayer aggregates are marked in light blue (one contour line), green (two lines), and yellow colors (three lines), respectively. The four panels are the 1st (a), 3rd (b), 10th (c), and 14th (d) frame selected from a 120 min image series. The evolution in the apparent height of selected Au aggregates is depicted in the two diagrams shown in (e) and (f). Note that some structures remain stable, while others frequently change their configuration upon scanning.

With increasing exposure, the number of Au aggregates on the surface keeps rising until saturation of the cluster density is observed at 0.03 ML nominal coverage (Figure 1c). The maximum cluster density at this condition amounts to $5 \times 10^{12} \text{ cm}^{-2}$ (Figure 1d), which is two times larger than the density of surface defects ($2.5 \times 10^{12} \text{ cm}^{-2}$) and indicates that the Au atoms are not only stabilized via heterogeneous nucleation on O defects. Competing processes might be homogeneous nucleation on the ideal surface, being favored by the limited mobility of Au atoms at 10 K deposition temperature, and heterogeneous nucleation on defects that are invisible in the STM, such as Ce³⁺ ions. If homogeneous nucleation would be the primary pathway, the mean distance between the Au aggregates of about $\sim 40 \text{ \AA}$ could be taken as a measure for the transient diffusion length of hot Au atoms impinging on the cold ceria surface. This relatively small value readily explains why step edges are only sparsely populated in our experiment, although they dominate the nucleation at room temperature.¹⁵

In the low coverage regime studied here, the Au aggregates still exhibit discrete height values indicative for an integer number of atomic planes. This fact can be visualized in color-coded STM images, in which monolayer species, e.g., monomers and flat islands, appear blue (one contour ring), while bilayer and trilayer clusters are depicted in green (two rings) and yellow (three rings), respectively (Figure 4a–d). The use of this color representation allows us to follow structural changes on the surface over large time frames (120 min). Evidently, the Au aggregates undergo a structure evolution during scanning, in which they change their position and/or appearance on the ceria film. To illustrate this fluxionality, we have chosen ten species (marked A–J) and followed their height evolution throughout the series (Figure 4e,f). While some species remained stable during the entire experiment, e.g., the monomers I and J and the bilayer pyramid G, others frequently switched configurations. The bilayer pyramid D, for example, loses most of its atoms in frame 9 and turns into a monomer, while adatom E accumulates atoms and grows in size. Some aggregates even change appearance repeatedly and seem to have a bistable configuration (e.g., cluster A). These instabilities can be identified even in single

images, as the corresponding aggregates exhibit a streaky appearance due to rapid restructurings occurring within a few scan lines. We can only speculate on the nature of this low-temperature fluxionality of Au aggregates on the CeO₂(111). Possible scenarios are:

- (i) Various iso-energetic configurations exist for a given cluster size, and transitions between them are induced by inelastically tunneling electrons from the tip. Gas-phase experiments have demonstrated the sometimes enormous configuration space of ultrasmall aggregates.³²
- (ii) The Au clusters are subject to continuous charging and discharging events, triggered either by electron injection from the tip³³ or charge exchange with the ceria support.^{16,18} As the charge state influences the electronic properties, hence the imaging contrast, the clusters rapidly change appearance in the STM.
- (iii) Gold atoms might be transferred from the surface to the tip apex, from where they get redeposited at another surface location after a couple of scan lines. The latter process might be enhanced by traces of CO molecules on the surface that are known to act as transporters for single Au atoms.^{13,34}

Two additional observations are worth mentioning in this context. First, smaller entities seem to be more stable than larger ones, as they exhibit a reduced configurational space and might be pinned to surface defects. Second, the tip-induced adatom motion does not lead to an overall increase of the cluster diameter, although larger aggregates are expected to be thermodynamically preferred with respect to smaller ones. We suggest that sintering effects are partially inhibited by clusters in particularly stable geometries (magic sizes) or energy barriers for the coalescence of neighboring aggregates. A better understanding of the role of the STM tip on the observed fluxionality requires insight into the stability of certain cluster geometries and into the mechanism of excitation transfer from tip electrons to the Au deposits.

3.2. Electronic Structure of the Au Aggregates. In the last paragraph, we discuss the electronic properties of small Au aggregates on the CeO₂ surface, as probed with dI/dV

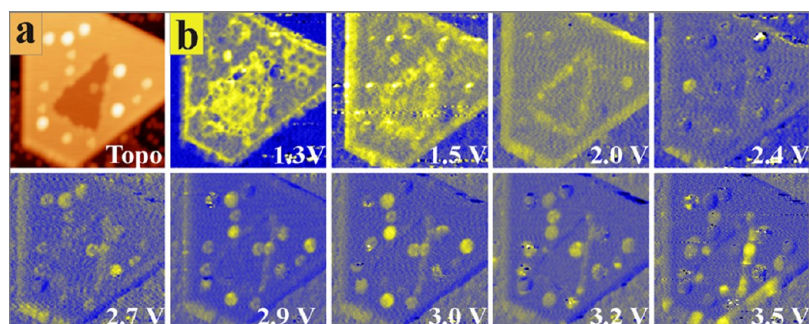


Figure 5. (a) STM topographic image and (b) corresponding dI/dV maps of a hexagonal $\text{CeO}_2(111)$ island covered with different Au aggregates. The applied bias voltage is given in the panels ($30 \times 30 \text{ nm}^2$).

spectroscopy and imaging. We have restricted our measurements to positive sample bias because of experimental difficulties to obtain filled state images and spectra on the insulating oxide film. Figure 5 shows a topographic image and a series of dI/dV maps taken on a hexagonal oxide island covered with a number of characteristic Au aggregates. The low bias maps (1.3–2.0 V) are dominated by conductance channels into the oxide, while the Au clusters hardly give any dI/dV response. Tunneling into pristine ceria is mediated by the empty Ce 4f band that provides final states for the tip electrons in this energy range despite the spatial localization of the f-orbitals.^{21,25} The signature of the 4f band also appears in the spectroscopic mode as a broad maximum centered at 2.3 eV (Figure 6a).

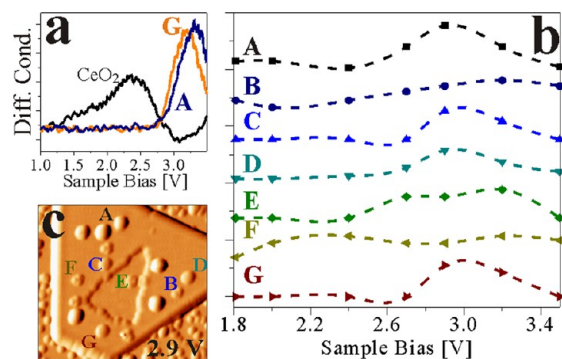


Figure 6. (a) Differential conductance spectra of bare ceria (black) and two Au aggregates (orange, blue) taken at 3.3 V bias set point. While the broad maximum on the oxide curve marks the Ce 4f band, the Au clusters show a peak at around 3.0 V that originates from the Au 6p-derived states. (b) dI/dV intensity of different Au clusters as deduced from the conductance maps shown in Figure 5. The respective aggregates are labeled in the topography image shown in (c) that has been differentiated to improve the contrast ($30 \times 30 \text{ nm}^2$).

Interestingly, the low-bias conductance maps display regular modulations with 19 Å periodicity that are invisible in the topographic mode. This hexagonal pattern relates to the (5×5) CeO_2 on the (7×7) Ru(0001) coincidence lattice, located at the metal–oxide interface.³⁵ Additional inhomogeneities in the electronic structure are introduced by the oxide step edges that were shown to expose distinct 1D edge states due to the lower atom coordination and residual step dipoles.²⁷

The Au aggregates become electronically active beyond 2.5 V, when they display enhanced contrast in the dI/dV maps. The maximum dI/dV signal with respect to the ceria background thereby occurs at different bias values for different clusters. To visualize this trend, we have plotted the bias-

dependent dI/dV intensity for seven Au clusters taken from Figure 5 (Figure 6b). Most of the larger aggregates (No. A, C, G) feature a broad maximum at 3.0 V, a finding that is corroborated by the dI/dV spectra shown in Figure 6a. In these curves, only the Au-induced states are detected, as the large tip–sample distance above the clusters renders the Ce 4f band invisible. Smaller aggregates display a more variable spectral response, e.g., a double peak for a pentamer (No. E), a low-bias resonance for the trimer (No. F), and no maximum at all for the dimer (No. B). Note that the dI/dV fingerprints are governed not only by the atom count but also by the different binding sites of the aggregates on the surface. This interplay between the intrinsic cluster electronic structure and the Au–ceria coupling makes a detailed discussion of the spectroscopic data difficult at this point.

Some general conclusions may still be drawn by comparing the present data with earlier Au spectra taken on alumina and magnesia supports.^{18,31} In those studies, the Au 6s states that usually provide the strongest dI/dV signal due to their delocalized nature were detected either below or close to the Fermi level, hence outside the spectral window accessed here (1.0–4.0 eV). Assuming a similar low-bias position of the Au 6s orbitals in ceria-supported deposits, we associate the dI/dV maxima around 3.0 V to the Au 6p states.³⁶ In contrast to the free-electron-like s states, the 6p orbitals feature a rather weak dispersion, and the broad dI/dV maxima observed here might therefore arise from the superposition of several p levels. The line width would further increase, if the actual Au resonances are dressed by phonon side bands of the ceria film. A similar effect has been used to explain the broad dI/dV peaks observed for Cl defects in ultrathin NaCl films.³⁷ A better characterization of the Au electronic structure would require the preparation of thinner ceria films, which enable spectroscopic measurements even at negative bias, hence in the region of the Au 6s states. However, also the characteristic bulk properties of ceria will disappear in this case. STM spectroscopy on oxides is therefore always a trade-off between facilitating tunneling transport by using thin films and increasing the thickness to establish a bulk-like environment for the adsorbates under investigation.

4. CONCLUSIONS

Using scanning tunneling microscopy and spectroscopy, we have analyzed the nucleation and growth behavior of gold on weakly reduced and defect-poor $\text{CeO}_2(111)$ films. On the ideal surface, single Au atoms bind to oxygen top or bridge sites, while step edges play only a minor role. With increasing Au exposure, upright standing dimers, bilayer and trilayer pyramids

develop on the surface. A clear trend for the vertical growth of gold indicates a close-to-neutral charge state of the aggregates, as negatively charged gold is known to prefer 2D island shapes. This conclusion is supported by the absence of other characteristic fingerprints of charged species in our experiment, e.g., of sombrero rings around the adatoms and a retarded aggregation at higher exposure.³⁸ Also conductance spectra of the Au aggregates could not provide evidence for a charge transfer but mainly revealed the spectral signature of Au 6p states well above the Fermi level. We therefore conclude that Au atoms and clusters adsorb to defect-poor CeO₂ surfaces in a close-to-neutral state. This picture may change on reduced films with a high density of Ce³⁺ defects, where charge transfer into the gold becomes easier. We will address this question in future work.

AUTHOR INFORMATION

Corresponding Author

*Tel.: +49-30-8413-4191. Fax: +49-30-8413-4100. E-mail: nilius@fhi-berlin.mpg.de.

Notes

The authors declare no competing financial interest.

ACKNOWLEDGMENTS

Y.C. thanks the Humboldt foundation for a fellowship. Support from the DFG within the Cluster of Excellence 'UniCat' is gratefully acknowledged.

REFERENCES

- (1) Rodriguez, J. A. Gold-based Catalysts for the Water–Gas Shift Reaction: Active sites and Reaction Mechanism. *Catal. Today* **2011**, *160*, 3–10.
- (2) Fu, Q.; Weber, A.; Flytzani-Stephanopoulos, M. Nanostructured Au–CeO₂ Catalysts for Low-Temperature Water-Gas Shift Reaction. *Catal. Lett.* **2001**, *77*, 87–95.
- (3) Deluga, G. A.; Salge, J. R.; Schmidt, L. D.; Verykios, X. E. Renewable Hydrogen from Ethanol by Autothermal Reforming. *Science* **2004**, *303*, 993–997.
- (4) Fu, Q.; Saltsburg, H.; Flytzani-Stephanopoulos, M. Active non-metallic Au and Pt Species on Ceria-based Water-gas shift Catalysts. *Science* **2003**, *301*, 935–938.
- (5) Zhang, C.; Michaelides, A.; Jenkins, S. J. Theory of Gold on Ceria. *Phys. Chem. Chem. Phys.* **2011**, *13*, 22–33.
- (6) Paier, J.; Penschke, C.; Sauer, J. Oxygen Defects and Surface Chemistry of Ceria: Quantum Chemical Studies Compared to Experiment. *Chem. Rev.* **2013**, *113*, 3949–3985.
- (7) Loschen, C.; Carrasco, J.; Neyman, K. M.; Illas, F. First Principles LDA+U and GGA+U Study of Cerium Oxides: Dependence on the Effective U-Parameter. *Phys. Rev. B* **2007**, *75*, 035115.
- (8) Nolan, M.; Grigoleit, S.; Sayle, D. C.; Parker, S. C.; Watson, G. W. Density Functional Theory Studies of the Structure and Electronic Structure of Pure and Defective low index surfaces of ceria. *Surf. Sci.* **2005**, *576*, 217–229.
- (9) Branda, M. M.; Castellani, N. J.; Grau-Crespo, R.; de Leeuw, N. H.; Hernández, N. C.; Sanz, J. F.; Neyman, K. M.; Illas, F. On the Difficulties of Present Theoretical Models to Predict the Oxidation State of Atomic Au Adsorbed on Regular Sites of CeO₂(111). *J. Chem. Phys.* **2009**, *131*, 094702.
- (10) Chen, Y.; Hu, P.; Lee, M. H.; Wang, H. Au on (1 1 1) and (1 1 0) surfaces of CeO₂: A Density-Functional Theory Study. *Surf. Sci.* **2008**, *602*, 1736–1741.
- (11) Hernandez, N. C.; Grau-Crespo, R.; de Leeuw, N. H.; Sanz, J. F. Electronic Charge Transfer between Ceria Surfaces and Gold Adatoms: a GGA+U Investigation. *Phys. Chem. Chem. Phys.* **2009**, *11*, 5246–5252.

(12) Camellone, M. F.; Fabris, S. Reaction Mechanisms for the CO Oxidation on Au/CeO₂ catalysts: Activity of Substitutional Au³⁺/Au⁺ Cations and Deactivation of Supported Au+ Adatoms. *J. Am. Chem. Soc.* **2009**, *131*, 10473–10483.

(13) Ghosh, P.; Camellone, M. F.; Fabris, S. Fluxionality of Au Clusters at Ceria Surfaces during CO Oxidation: Relationships among Reactivity, Size, Cohesion, and Surface Defects from DFT Simulations. *J. Phys. Chem. Lett.* **2013**, *4*, 2256–2263.

(14) Zhao, X.; Ma, S.; Hrbek, J.; Rodriguez, J. A. Reaction of water with Ce–Au(1 1 1) and CeO_x/Au(1 1 1) surfaces: Photoemission and STM studies. *Surf. Sci.* **2007**, *601*, 2445–2452.

(15) Lu, J.-L.; Gao, H.-J.; Shaikhutdinov, S.; Freund, H.-J. Gold Supported on Well Ordered Ceria Films: Nucleation, Growth and Morphology in CO Oxidation Reaction. *Catal. Lett.* **2007**, *114*, 8–16.

(16) Baron, M.; Bondarchuk, O.; Stacchiola, D.; Shaikhutdinov, S.; Freund, H.-J. Interaction of Gold with Cerium Oxide Supports: CeO₂(111) Thin Films vs CeO_x Nanoparticles. *J. Phys. Chem. C* **2009**, *113*, 6042–6049.

(17) Giordano, L.; Pacchioni, G.; Goniakowski, J.; Nilus, N.; Rienks, E. D. L.; Freund, H.-J. Charging of Metal Adatoms on Ultrathin Oxide Films: Au and Pd on FeO/Pt(111). *Phys. Rev. Lett.* **2008**, *101*, 026102.

(18) Nilus, N.; Ganduglia-Pirovano, M. V.; Brázdová, V.; Kulawik, M.; Sauer, J.; Freund, H.-J. Electronic Properties and Charge State of Gold Monomers and Chains adsorbed on Alumina Thin Films on NiAl(110). *Phys. Rev. B* **2010**, *81*, 045422.

(19) Mullins, D. R.; Radulovic, P. V.; Overbury, S. H. Ordered Cerium Oxide Thin Films Grown on Ru(0001) and Ni(111). *Surf. Sci.* **1999**, *429*, 186–198.

(20) Mullins, D. R.; Kundakovic, L.; Overbury, S. H. The Interaction between NO and CO on Rh-Loaded CeO_x(111). *J. Catal.* **2000**, *195*, 169–179.

(21) Shao, X.; Jerratsch, J.-F.; Nilus, N.; Freund, H.-J. Probing the 4f states of Ceria by Tunneling Spectroscopy. *Phys. Chem. Chem. Phys.* **2011**, *13*, 12646–12651.

(22) Esch, F.; Fabris, S.; Zhou, L.; Montini, T.; Africh, C.; Fornasiero, P.; Comelli, G.; Rosei, R. Electron Localization Determines Defect Formation on Ceria Substrates. *Science* **2005**, *309*, 752–755.

(23) Torbrügge, S.; Reichling, M.; Ishiyama, A.; Morita, S.; Custance, Ó. Evidence of Subsurface Oxygen Vacancy Ordering on Reduced CeO₂(111). *Phys. Rev. Lett.* **2007**, *99*, 056101.

(24) Torbrügge, S.; Cranney, M.; Reichling, M. Morphology of Step Structures on CeO₂(111). *Appl. Phys. Lett.* **2008**, *93*, 073112.

(25) Jerratsch, J.-F.; Shao, X.; Nilus, N.; Freund, H.-J.; Cristina, P.; Sauer, J. Electron Localization in Defective Ceria Films: A Study with Scanning-Tunneling Microscopy and Density-Functional Theory. *Phys. Rev. Lett.* **2011**, *106*, 246801.

(26) Grinter, D. C.; Ithnin, R.; Pang, C. L.; Thornton, G. Defect Structure of Ultrathin Ceria Films on Pt(111): Atomic Views from Scanning Tunneling Microscopy. *J. Phys. Chem. C* **2010**, *114*, 17036–17041.

(27) Nilus, N.; Kozlov, S. M.; Jerratsch, J.-F.; Baron, M.; Shao, X.; Vines, F.; Shaikhutdinov, S.; Neyman, K. M.; Freund, H.-J. Formation of One-dimensional Electronic States along the Step Edges of CeO₂(111). *ACS Nano* **2012**, *6*, 1126–1133.

(28) Zhang, C.; Michaelides, A.; King, D. A.; Jenkins, S. J. Structure of Gold Atoms on Stoichiometric and Defective Ceria Surfaces. *J. Chem. Phys.* **2008**, *129*, 194708.

(29) Simic-Milosevic, V.; Heyde, M.; Nilus, N.; König, T.; Rust, H.-P.; Sterrer, M.; Risse, T.; Freund, H.-J.; Giordano, L.; Pacchioni, G. Au Dimers on Thin MgO(001) Films: Flat and Charged or Upright and Neutral? *J. Am. Chem. Soc.* **2008**, *130*, 7814–7815.

(30) Del Vitto, A.; Pacchioni, G.; Delbecq, F. O.; Sautet, P. Au Atoms and Dimers on the MgO(100) surface: a DFT Study of Nucleation at Defects. *J. Phys. Chem. B* **2005**, *109*, 8040–8048.

(31) Simic-Milosevic, V.; Heyde, M.; Lin, X.; König, T.; Rust, H.-P.; Sterrer, M.; Risse, T.; Nilus, N.; Freund, H.-J.; Giordano, L.; Pacchioni, G. Charge-induced Formation of Linear Au Clusters on Thin MgO Films: Scanning Tunneling Microscopy and Density-Functional Theory Study. *Phys. Rev. B* **2008**, *78*, 235429.

(32) Gruene, P.; Rayner, D. M.; Redlich, B.; van der Meer, A. F.; Lyon, J. T.; Meijer, G.; Fielicke, A. Structures of Neutral Au₇, Au₁₉, and Au₂₀ Clusters in the Gas Phase. *Science* **2008**, *321*, 674–676.

(33) Repp, J.; Meyer, G.; Olson, F. E.; Persson, M. Controlling the Charge State of Individual Gold Adatoms. *Science* **2004**, *305*, 493–495.

(34) Parkinson, G. S.; Novotny, Z.; Argentero, G.; Schmid, M.; Pavelec, J.; Kosak, R.; Blaha, P.; Diebold, U. Carbon Monoxide-induced Adatom Sintering in a Pd–Fe₃O₄ Model Catalyst. *Nat. Mater.* **2013**, *12*, 724–728.

(35) Castellarin-Cudia, C.; Surnev, S.; Schneider, G.; Podlucky, R.; Ramsey, M. G.; Netzer, F. P. Strain-induced Formation of Arrays of Catalytically Active Sites at the Metal–oxide Interface. *Surf. Sci.* **2004**, *554*, L120–L126.

(36) Lin, X.; Nilius, N.; Sterrer, M.; Koskinen, P.; Häkkinen, H.; Freund, H.-J. Characterizing Low-coordinated Atoms at the Periphery of MgO-supported Au Islands using Scanning Tunneling Microscopy and Electronic Structure Calculations. *Phys. Rev. B* **2010**, *81*, 153406.

(37) Repp, J.; Meyer, G.; Paavilainen, S.; Olson, F. E.; Persson, M. Scanning Tunneling Spectroscopy of Cl Vacancies in NaCl Films: Strong Electron-Phonon Coupling in Double-Barrier Tunneling Junctions. *Phys. Rev. Lett.* **2005**, *95*, 225503.

(38) Sterrer, M.; Risse, T.; Martinez Pozzoni, U.; Giordano, L.; Heyde, M.; Rust, H.-P.; Pacchioni, G.; Freund, H.-J. Control of the Charge State of Metal Atoms on Thin MgO Films. *Phys. Rev. Lett.* **2007**, *98*, 096107.

■ NOTE ADDED AFTER ASAP PUBLICATION

This paper was published ASAP on October 14, 2013, with an error to the Authors. The corrected version was reposted October 15, 2013.